Sentinel-1A Assessment Results from the Use of Permanent SAR Corner Reflectors in Cyprus by means of the CyCLOPS Strategic Infrastructure

Dimitris Kakoullis*[a], Kyriaki Fotiou[a,b], Nerea Ibarrola Subiza[c], Ramon Brcic[c], Michael Eineder[c], Chris Danezis[a,b]

[a]Cyprus University of Technology, Department of Civil Engineering & Geomatics, P.O. BOX 50329, 3036, Limassol, Cyprus; [b]ERATOSTHENES Centre of Excellence, Limassol, 3012, Cyprus; [c]SAR Signal Processing Department, German Aerospace Center, Wessling, 82234, Germany

*dimitris.kakoullis@cut.ac.cy; www.celestia.eu; www.cyclops.cy

ABSTRACT

CyCLOPS (Cyprus Continuously Operating Natural Hazards Monitoring and Prevention System) plays a pivotal role in geophysical and geotechnical monitoring in Cyprus and the EMMENA region. This strategic research infrastructure comprises six permanent stations, each with a Tier-1 GNSS reference station and two calibration-grade corner reflectors (CRs) of 1.5m inner length. CRs are oriented to the ESA's Sentinel-1 satellite mission to account for ascending and descending tracks. Since reaching full operational status in June 2021, CyCLOPS has been instrumental in observing geodynamic phenomena and landslide activities in Cyprus. This study analyses Sentinel-1A SAR performance by exploiting the CyCLOPS network to estimate key parameters such as spatial resolution, side-lobe levels, Radar Cross-Section (RCS), Signal-to-Clutter Ratio (SCR), phase stability, and localization accuracy. Results demonstrate the effectiveness of the CyCLOPS infrastructure in maintaining high-quality SAR imagery radiometric parameters, with consistent spatial resolution, controlled side-lobe levels, and reliable RCS and SCR values closely aligned with theoretical expectations. Furthermore, localization analysis has proven effective in mitigating atmospheric and dynamic Earth influences, ensuring geolocation accuracy. Consequently, the CyCLOPS infrastructure is a state-of-the-art, reliable unit for radiometric calibration and validation of SAR products, which will contribute to the precision and reliability of SAR imaging, crucial for various applications such as crustal motion monitoring.

Keywords: Sentinel-1A, Corner Reflectors, Radiometric Calibration, Geolocation Analysis

1. INTRODUCTION

CyCLOPS consists of a comprehensive multi-parametric network spread across the government-controlled region of Cyprus, along with an Operation Centre. The permanent segment, illustrated in Figure 1, features six sites, each equipped with a Tier-1 GNSS continuously operating reference station (CORS) and two calibration-grade triangular trihedral corner reflectors (CRs) with an inner length of 1.5 meters. These are designed to support both the ascending and descending tracks of Synthetic Aperture Radar (SAR) satellite missions, such as ESA's Sentinel-1 [1]. The site selection was guided by a GIS-based methodology developed by the CUT Laboratory of Geodesy [2], adhering to stringent international standards [3–5], thereby ensuring the network's capability for precise crustal movement monitoring and enhancing SAR data.

For precise deformation monitoring using SAR acquisitions, external calibration is crucial. This involves the use of ground targets like corner reflectors (CRs), which are artificial persistent scatterers, with known Radar Cross Section (RCS), to ensure effective system calibration [6,7]. Radiometric calibration is achieved by comparing the observed backscatter signal intensity from CRs with their theoretical RCS (RCS_T) [8], thus allowing the determination of an absolute calibration factor [9]. The goal is to establish an absolute calibration factor by associating SAR image pixel values with precise geophysical parameters, ensuring the imagery's precision and utility for various applications [10].

Geolocation accuracy refers to the precision with which an Earth-observing remote sensing platform can determine the geographic positions of surface features in its images [11]. By comparing the surveyed in-situ coordinates of CRs to the actual location of its peak intensity within a specific image, one can determine an offset, accounting for system biases, and

Tenth International Conference on Remote Sensing and Geoinformation of the Environment (RSCy2024), edited by A. Christofe, S. Michaelides, D. Hadjimitsis, C. Danezis, K. Themistocleous, N. Kyriakides, G. Schreier,
Proc. of SPIE Vol. 13212, 132120R · © 2024 SPIE · 0277-786X · doi: 10.1117/12.3037227

effects such as atmospheric path delay, plate tectonics, and solid Earth tide (SET) disturbances [12]. Concordantly, the collocation of CRs with GNSS CORS enhances the calibration process, evidently leading to greater accuracy in estimating interferometric phases and producing more reliable deformation products [13].

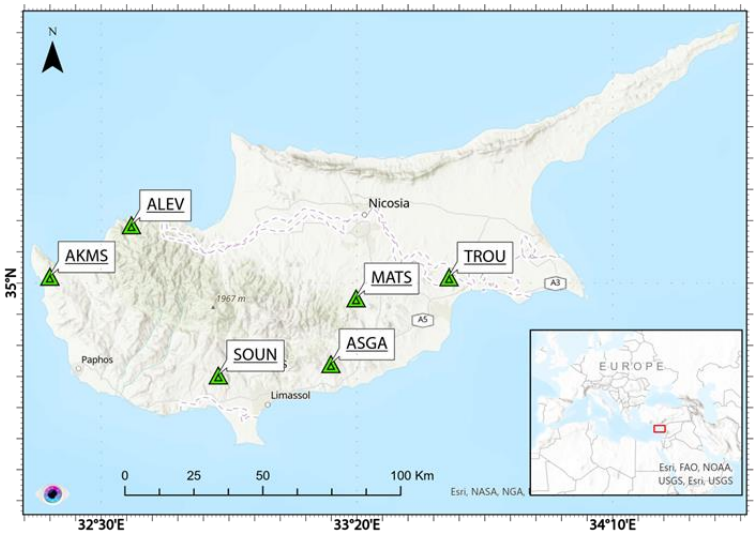

Figure 1. The CyCLOPS permanent network [2]. Green triangles denote the collocated GNSS CORS and CR sites.

The objective of this paper is to present the initial results of assessing ESA Sentinel-1A (S1A) SAR performance using the response from CyCLOPS CRs. The structure is as follows: Sections 2, 3, and 4 outline the procedure used to assess CRs in terms of radiometric parameters, while Section 5 derives the Absolute Location Error (ALE) of SAR products.

This paper summarizes key findings and methodologies that are part of a more extensive work published in [14]. For a more detailed analysis and comprehensive discussion, readers are encouraged to refer to the journal article.

2. IMPULSE RESPONSE FUNCTION

The Impulse Response Function (IRF) in SAR imaging, also known as the point-spread function, depicts the two-dimensional luminosity pattern of a point scatterer such as a CR or transponder in focused images. The 3 dB width of the IRF determines the spatial resolution, while the sidelobes provide insights into the performance of the SAR instrument and processor. Key image quality metrics include spatial resolution (3 dB width of the peak lobe), Peak Side-Lobe Ratio (PSLR), and Integrated Side-Lobe Ratio (ISLR), all derived from the point target's IRF [7]. Table 1 lists standard S1 Interferometric Wide Swath (IW) Level-1 SLC product characteristics as defined in the ESA S1 product definition [15].

Table 1. S1 IW SLC product performance parameters.

Parameters	IW1	IW2	IW3
PSLR in range and azimuth [dB]	< -21.2	< -21.2	< -21.2
ISLR in range and azimuth [dB]	< -16.1	< -16.1	< -16.1
Slant Range resolution [m]	2.7	3.1	3.5
Azimuth resolution [m]	22.5	22.7	22.6

The actual image quality performance was assessed through a temporal evaluation of the CRs' responses within the SLC images. A total of twenty-six Level-1 uncalibrated intensity images with linear vertical polarization (VV) from 29.06.2021 to 18.10.2023 were used to periodically monitor the consistency and stability of the quality parameters. Subsequently, the IRF parameters in both range and azimuth for each CR were calculated as defined in the CEOS standard definition, using the GAMMA software package [16]. The IRF for each CR in all acquired images was generated by applying the integral method [17], keeping the clutter window size as large as the window used for extracting the point target to maintain result reliability. The peak of the point target is situated at the central pixel of the data segment, as identified by the image coordinates. The images were oversampled by a factor of 16, resulting in an oversampled point target image with dimensions of 256x256, originating from a 16x16 image. Consequently, the dimensions of the interpolated image are dictated by the magnitude of the oversampling factor. Finally, the temporal variation of the spatial resolution, PSLR, and ISLR from each CR is obtained.

Figure 2 illustrates a representative example of the TROU01 CR impulse response. Among the three parameters mentioned, spatial resolution, which refers to the minimum distance at which two distinct objects on the ground surface can be discerned as separate entities in an image, is the most critical in assessing image quality [18].

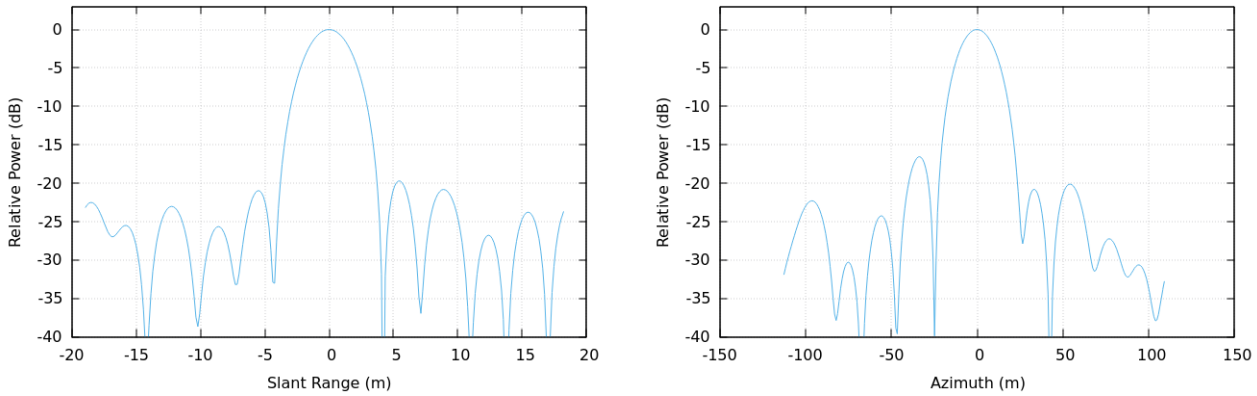

(a) (b)

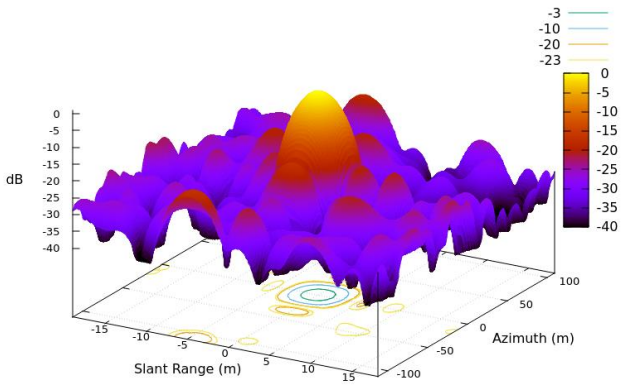

(c)

Figure 2. The TROU01 CR response function, after interpolation, in the S1A - IW3 - VV image of 23/09/2023 ascending pass. (a) and (b) plots represent a cut through the peak in the slant range and azimuth direction, respectively, while (c) illustrates the point target relative power in a 3D plot.

Spatial Resolution in SAR Imaging

Spatial resolution in range and azimuth directions is defined by the width of two points at the −3 dB mainlobe [7] . As shown in Figures 2a and 2b, for instance, a relative power of −3 dB (y-axis) represents a width of 3.5 m and 22.4 m (x-axis) in range and azimuth, respectively. Figure 3 illustrates the temporal variation of spatial resolution from the TROU01 CR.

Temporal analysis indicates consistent and reliable spatial resolution, aligning with S1A's IW3 swath specifications. Assessments across IW1, IW2, and IW3 swaths (see Table 2) reveal that CRs' responses maintain consistency with theoretical slant range and azimuth resolutions.

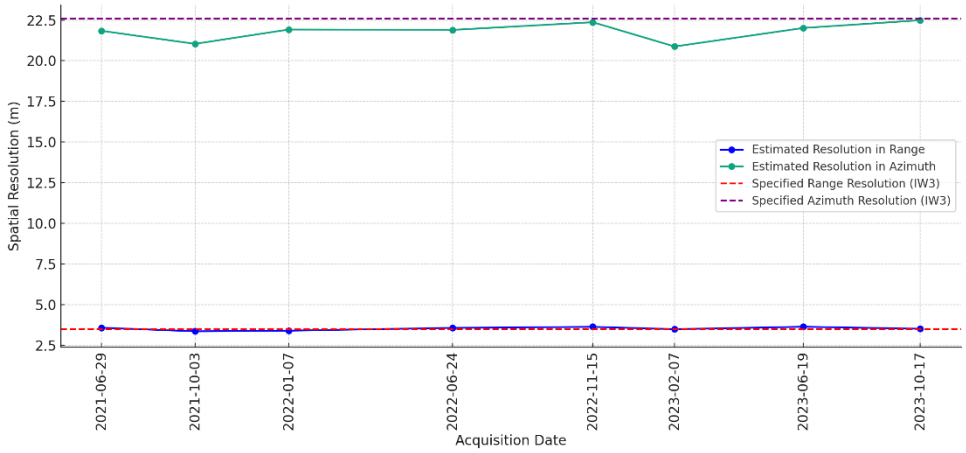

Figure 3. The temporal variation of spatial resolution from TROU01 CR, for the monitoring period.

Discrepancies exceeding theoretical values suggest potential processing issues, such as inaccurate orbit data [19].

Table 2. Statistics of Spatial Resolution Quality Assessment from all the twelve (12) CRs.

	Range [m]	**Azimuth [m]**
IW1		
Mean	2.7	21.9
St. Deviation	0.09	0.5
Max	2.8	22.8
Min	2.5	20.8
IW2		
Mean	3.1	22.1
St. Deviation	0.09	0.6
Max	3.3	23.5
Min	2.9	21.2
IW3		
Mean	3.5	21.8
St. Deviation	0.09	0.5
Max	3.7	22.8
Min	3.4	20.8

Sidelobe Level

Controlling the intensity of the sidelobes is another critical parameter, measured and compared against theoretical values. PSLR is defined as the ratio of the maximum (peak) intensity of the main lobe to that of the most intense side-lobe in the IRF, representing the contrast or clarity between adjacent point targets [7]. ISLR, the third image quality estimate, is defined as the ratio of the side-lobe energy to the main lobe energy of the response, indicating the capability to detect a weak target's response near highly reflective targets. ISLR measures the relative reflectance of the sidelobes in comparison to the main lobe, providing an assessment of overall image quality and target distinguishability [20]. Table 3 provides the statistics of the ISLR estimation from all CRs.

Table 3. Statistics of ISLR Quality Measurements from all the twelve (12) CRs.

	Range [dB]	**Azimuth [dB]**
Mean	−19.3	−20.2
St. Deviation	2.2	3.4
Max	−15	−13.6
Min	−25.8	−34.8

3. RCS AND SCR ESTIMATION

To ensure sufficient visibility of point targets above the surrounding background clutter, it's essential to evaluate the target size as observed in SAR images. This evaluation is achieved through the estimation of the RCS of the CRs, which measures the amount of energy backscattered by a target. Additionally, the visibility of CRs above the clutter is determined by the Signal to Clutter Ratio (SCR), calculated as the ratio of the CR's RCS to the clutter RCS. RCS estimation can be performed using either the integral method [17] or the peak method [21]. The peak method relies on the resolution parameters of the point targets, making its accuracy dependent on the quality of the point target image, such as clarity and focus, for precise calibration factor determination. In contrast, the integral method is independent of point target parameters [22]. The RCS of each CR was measured in every SAR image using both methods and compared to the theoretical value to calculate the mean RCS for evaluation.

The theoretical RCS at C-band for a triangular trihedral CR of 1.5 m is 38.38 dBm²; therefore, the estimated RCS values should not exceed this theoretical value [23]. Generally, for SAR images, the RCS of a triangular trihedral CR of 1.5 m suitable for radiometric calibration at C-band should range between 34 and 38 dBm² [24]. Regarding SCR requirements, a CR should provide high-intensity radar reflections in SAR images while maintaining a low level of surrounding scatterers' signal reflectivity, ensuring a high SCR. Thus, a high-intensity and temporally stable backscatter response is crucial for the correct identification of a CR in SAR images [25]. For a 1.5 m CR operating at C-band, the minimum suitable SCR for radiometric calibration should be at least 20 dB [24,26]. Even if the surrounding clutter is low, it should be estimated during the analysis, typically in the corners of the image chip, and subtracted from the signal estimate. Estimating the SCR also involves assessing factors such as phase stability.

A total of 195 Ground Range Detected (GRD) image products (IW swath, VV polarization), including both ascending and descending paths, from 17.06.2021 to 26.07.2023, were processed for RCS and SCR estimation using the integral method. The integral method can be used in multilook images. The responses of the CRs were calculated using CoRAL software, and the methodology followed is described in [27]. The mean estimated RCS is 37.58 ± 0.05 (1σ) dBm², which is a 0.8 dBm² difference from the RCST. The estimated mean SCR, assuming spatial ergodicity, is 24.23 ± 0.08 (1σ) dB.

For the peak calibration method, 297 SLC image products (IW swath, VV polarization), including both ascending and descending paths, from 22.06.2021 to 29.10.2023, were processed. The RCS and SCR estimation, assuming temporal ergodicity of the clutter, were extracted using GECORIS software, and the methodology followed is described in [28]. The mean RCS is 37.6 ± 0.03 (1σ) dBm², which is a 0.78 dBm² difference from the RCS_T, while the mean SCR is 27± 0.8 dB.

As shown in Figure 4, the mean estimated RCS difference between the two methods is 0.02 dBm², with the peak method's standard 1σ error being smaller than that of the integral method. These findings align with existing literature, indicating

that RMS errors associated with the peak method are consistently smaller than or at least equal to those of the integral method in well-focused systems [21].

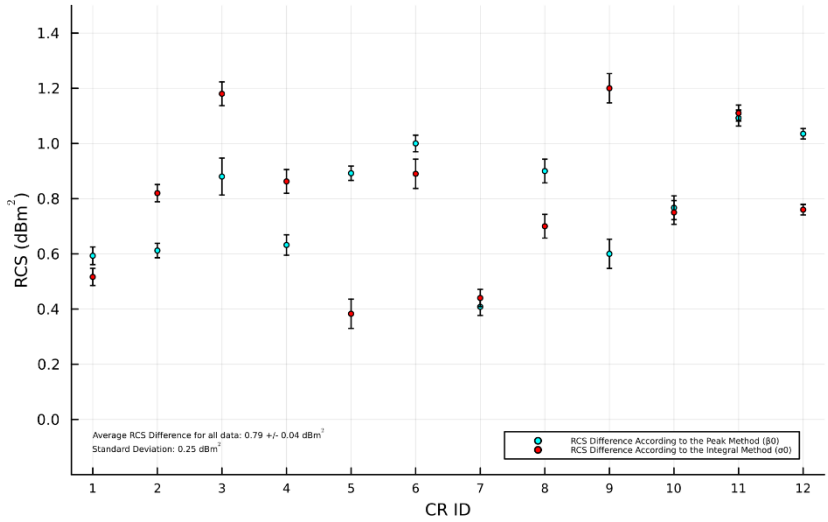

Figure 4. Estimated RCS difference from RCS_T for all the CRs using both methods.

4. SLANT DISTANCE ERROR IN LOS

The pixel value containing the CR results from a complex sum of the backscatter signal contributed by the CR, the dominant scatterer, and the distributed individual scatterers within the pixel. This clutter contribution results in an uncorrelated signal, and the probability density function for the phase error (φ) magnitude of a CR can be estimated by its SCR [24]. For accurate SAR image calibration using a CR, it is crucial to maintain the phase standard deviation below 0.25 radians to ensure that phase residuals are normally distributed, and the SCR phase variance estimate remains unbiased [24–26,29,30]. By using λ, the φ angle's radians can be converted into a Line of Sight (LoS) slant distance error. For an SCR of 20 dB, the theoretical dispersion threshold for the LoS displacement error in C-band is approximately 0.31 mm. Figure 5 illustrates the average LoS distance error for each CR, where phase stability ranges from 0.04 to 0.05 radians, and all values lie below the aforementioned threshold, varying between 0.17 mm and 0.21 mm.

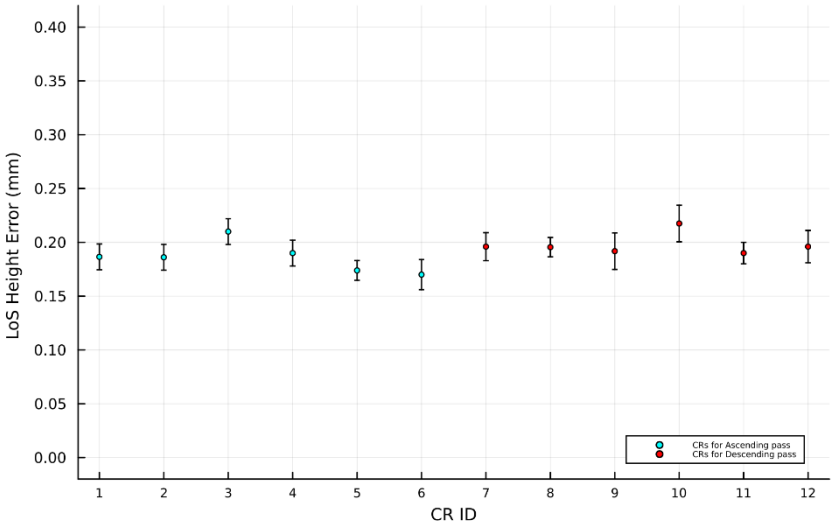

Figure 5. Mean displacement error in LoS.

5. GEOLOCATION ANALYSIS

Another critical aspect of assessing SAR image quality is geometric calibration, where pixel coordinates are compared to well-known locations of reference point targets, such as CRs, whose positions have been surveyed using adequate GNSS receivers. Due to accurate time and precise orbit determination, SAR images demonstrate sufficient geometric accuracy. However, these measurements are susceptible to factors such as variable atmospheric conditions, Earth dynamics, and approximations made during SAR processing. These influences can introduce apparent displacement shifts, occasionally reaching several meters. Mitigating these influences requires several post-processing steps and external data for accurate correction [31].

For each CR, a fixed reference point (RP) below the CR apex (phase center) was surveyed using GNSS static measurements, considering the height offsets between the RP and the apex. Their 3D coordinate positions were corrected with respect to the coordinates of the co-located CyCLOPS GNSS/CORS at each site, in ITRF 2014. Using GECORIS software, ALE for each CR was extracted. A representative example of the timing corrections can be seen in Figure 6, where the mean ALE in TROU01 is -0.029 ± 0.046 m, and -0.198 ± 0.287 m in range and azimuth, respectively.

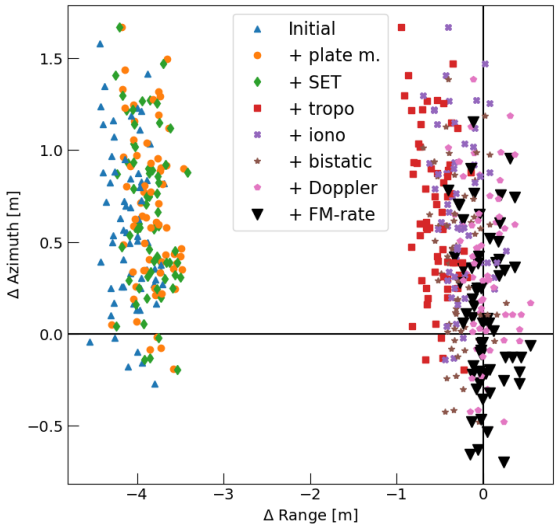

Figure 6. An example of the ALE estimation in TROU01 after mitigating the propagation influences. Blue triangles indicate the initial positions whereas black triangles are the final positions, in each acquisition.

6. CONCLUSIONS

The temporal analysis of IRF parameters, including spatial resolution, ISLR, indicated consistent and reliable performance of Sentinel-1A. The spatial resolution of CR responses aligned closely with the theoretical expectations for the IW swath, with minor discrepancies attributed to potential processing issues such as inaccurate orbit data.

Both the integral and peak methods for RCS estimation provided results close to the theoretical values, with mean estimated RCS values slightly below the RCS_T for a 1.5 m CR at C-band. The SCR estimates confirmed the high-intensity and stable backscatter response required for accurate CR identification in SAR imagery. Furthermore, the analysis of phase stability and corresponding slant distance errors in LoS ensured that the SCR phase variance remained unbiased, with average displacement errors in LoS well within acceptable limits.

Geometric calibration through comparison of pixel coordinates with surveyed CR positions revealed that geometric accuracy in SAR images is influenced from several factors such as atmospheric conditions and Earth dynamics which introduced potential displacement shifts, necessitating post-processing corrections. The ALE analysis has proven effective in mitigating atmospheric and dynamic Earth influences, ensuring localization accuracy.

Concordantly, the CyCLOPS infrastructure is a state-of-the-art, reliable unit for radiometric calibration and validation of SAR products, which will contribute significantly to the precision and reliability of SAR imaging, crucial for various applications such as crustal movement monitoring.

ACKNOWLEDGEMENTS

The authors would like to acknowledge the ‘CyCLOPS’ (RIF/INFRASTRUCTURES/1216/0050) project, which is funded by the European Regional and Development Fund and the Republic of Cyprus through the Research and Innovation Foundation in the framework of the RESTART 2016-2020 programme.

The authors would like to acknowledge the ‘CyCLOPS+’ (RIF/SMALL SCALE INFRASTRUCTURES/1222/0082) project, which is co-financed by the EU Structural Fund within the framework of the Cohesion Policy Programme "THALIA 2021-2027" and by national resources (Budget of the Cyprus University of Technology).

REFERENCES

[1] Danezis, C., Kakoullis, D., Fotiou, K., Pekri, M., Chatzinikos, M., Kotsakis, C., Brcic, R., Eineder, M., Nikolaidis, M., Ioannou, G., Christofe, A., Kyriakides, N., Melillos, G., Christoforou, M., Tzouvaras, M., Pilidou, S., Themistocleous, K. and Hadjimitsis, D., “CyCLOPS: A National Integrated GNSS/InSAR Strategic Research Infrastructure for Monitoring Geohazards and Forming the Next Generation Datum of the Republic of Cyprus,” Springer, Berlin, Heidelberg, 1–14.

[2] Kakoullis, D., Fotiou, K., Melillos, G. and Danezis, C., “Considerations and Multi-Criteria Decision Analysis for the Installation of Collocated Permanent GNSS and SAR Infrastructures for Continuous Space-Based Monitoring of Natural Hazards,” 4, Remote Sensing **14**(4), 1020 (2022).

[3] IGS., “IGS site guidelines,” Infrastructure Commitee, Central Bureau, Pasadena, CA, USA (2015).

[4] NGS., “Guidelines for New and Existing Continuously Operating Reference Stations (CORS),” NOAA, Silver Spring, 21 (2018).

[5] EUREF Permanent GNSS Network Central Bureau., “Guidelines for EPN Stations and Operational Centres” (2022).

[6] Garthwaite, M. C., Hazelwood, M., Nancarrow, S., Hislop, A. and Dawson, J. H., “A regional geodetic network to monitor ground surface response to resource extraction in the northern Surat Basin, Queensland,” Australian Journal of Earth Sciences **62**(4), 469–477 (2015).

[7] Freeman, A., “SAR calibration: an overview,” IEEE Transactions on Geoscience and Remote Sensing **30**(6), 1107–1121 (1992).

[8] ESA., “External Calibration,” <https://sentinel.esa.int/web/sentinel/technical-guides/sentinel-1-sar/cal-val-activities/calibration/external>.

[9] Freeman, A., "Radiometric calibration of SAR image data," International archives of photogrammetry and remote sensing **29**, 212–212 (1993).
[10] Sharma, S., Dadhich, G., Rambhia, M., Mathur, A. K., Prajapati, R. P., Patel, P. R. and Shukla, A., "Radiometric calibration stability assessment for the RISAT-1 SAR sensor using a deployed point target array at the Desalpar site, Rann of Kutch, India," International Journal of Remote Sensing **38**(23), 7242–7259 (2017).
[11] Schubert, A., Small, D., Miranda, N., Geudtner, D. and Meier, E., "Sentinel-1A Product Geolocation Accuracy: Commissioning Phase Results," 7, Remote Sensing **7**(7), 9431–9449 (2015).
[12] Schubert, A., Small, D., Meier, E., Miranda, N. and Geudtner, D., "Spaceborne SAR product geolocation accuracy: A Sentinel-1 update," 2014 IEEE Geoscience and Remote Sensing Symposium, 2675–2678 (2014).
[13] Mahapatra, P., Marel, H., Van Leijen, F., Samiei Esfahany, S., Klees, R. and Hanssen, R., "InSAR datum connection using GNSS-augmented radar transponders," Journal of Geodesy **92**, 21–32 (2017).
[14] Kakoullis, D., Fotiou, K., Ibarrola Subiza, N., Brcic, R., Eineder, M. and Danezis, C., "An Advanced Quality Assessment and Monitoring of ESA Sentinel-1 SAR Products via the CyCLOPS Infrastructure in the Southeastern Mediterranean Region," 10, Remote Sensing **16**(10), 1696 (2024).
[15] Bourbigot, M., "Sentinel-1 Product Definition" (2016).
[16] Wegmuller, U. and Werner, C., "GAMMA SAR processor and interferometry software," 3rd ERS Scientific Symposium, Florencen Italy (1997).
[17] Gray, A. L., Vachon, P. W., Livingstone, C. E. and Lukowski, T. I., "Synthetic aperture radar calibration using reference reflectors," IEEE Transactions on Geoscience and Remote Sensing **28**(3), 374–383 (1990).
[18] Dadhich, G., Sharma, S., Rambhia, M., Mathur, A. K., Patel, P. R. and Shukla, A., "Image quality characterization of fine resolution RISAT-1 data using impulse response function," Geocarto International **34**(6), 586–596 (2019).
[19] Small, D., "Flattening Gamma: Radiometric Terrain Correction for SAR Imagery," IEEE Trans. Geosci. Remote Sensing **49**(8), 3081–3093 (2011).
[20] Vu, V. T., Sjögren, T. K., Pettersson, M. I. and Gustavsson, A., "Definition on SAR image quality measurements for UWB SAR," Image and Signal Processing for Remote Sensing XIV **7109**, 367–375, SPIE (2008).
[21] Ulander, I. M. H., "Accuracy of using point targets for SAR calibration," IEEE Transactions on Aerospace and Electronic Systems **27**(1), 139–148 (1991).
[22] Praveen, T. N., Vinod Raju, M., Vishwanath, B. D., Meghana, P., Manjula, T. R. and Raju, G., "Absolute radiometric calibration of RISAT-1 SAR image using peak method," 2018 3rd IEEE International Conference on Recent Trends in Electronics, Information & Communication Technology (RTEICT), 456–460 (2018).
[23] Li, C., Zhao, J., Yin, J., Zhang, G. and Shan, X., "Analysis of RCS characteristic of dihedral corner and triangular trihedral corner reflectors," 2010 5th International Conference on Computer Science Education, 40–43 (2010).
[24] Garthwaite, M. C., Nancarrow, S., Hislop, A., Thankappan, M., Dawson, J. H. and Lawrie, S., [The Design of Radar Corner Reflectors for the Australian Geophysical Observing System: a single design suitable for InSAR deformation monitoring and SAR calibration at multiple microwave frequency bands.], Geoscience Australia, Canberra, Australia (2015).
[25] Qin, Y., Perissin, D. and Lei, L., "The Design and Experiments on Corner Reflectors for Urban Ground Deformation Monitoring in Hong Kong," International Journal of Antennas and Propagation **2013**, 1–8 (2013).
[26] Ferretti, A., Savio, G., Barzaghi, R., Borghi, A., Musazzi, S., Novali, F., Prati, C. and Rocca, F., "Submillimeter Accuracy of InSAR Time Series: Experimental Validation," IEEE Transactions on Geoscience and Remote Sensing **45**(5), 1142–1153 (2007).
[27] Garthwaite, M. C., "On the Design of Radar Corner Reflectors for Deformation Monitoring in Multi-Frequency InSAR," 7, Remote Sensing **9**(7), 648 (2017).
[28] Czikhardt, R., Van Der Marel, H. and Papco, J., "GECORIS: An Open-Source Toolbox for Analyzing Time Series of Corner Reflectors in InSAR Geodesy," Remote Sensing **13**(5), 926 (2021).
[29] Garthwaite, M. C., "On the Design of Radar Corner Reflectors for Deformation Monitoring in Multi-Frequency InSAR," 7, Remote Sensing **9**(7), 648 (2017).
[30] Ketelaar, G., Marinkovic, P. and Hanssen, R., "Validation of Point Scatterer Phase Statistics in Multi-Pass InSAR," [Envisat & ERS Symposium], ESA, Salzburg, Austria, 72.1 (2005).
[31] Gisinger, C., Krieger, L., Valentino, A., Breit, H., Albinet, C. and Eineder, M., "ESA's Extended Timing Annotation Dataset (ETAD) for Sentinel-1 - Product Status and Case Studies," presented at Living Planet Symposium, 23 May 2022, Bonn, ESA.